Study of ^{19}Na at SPIRAL

F. De Oliveira Santos, P. Himpe, M. Lewitowicz, I. Stefan, N. Smirnova, N.L. Achouri, J.C. Angélique, C. Angulo, L. Axelsson, D. Baiborodin, et al.

EPJ manuscript No.
(will be inserted by the editor)

Study of ^{19}Na at SPIRAL

F. de Oliveira Santos[1], P. Himpe[1,2], M. Lewitowicz[1], I. Stefan[1,8], N. Smirnova[2], N.L. Achouri[3], J.C. Angélique[3], C. Angulo[4], L. Axelsson[14], D. Baiborodin[6], F. Becker[1], M. Bellegui[5], E. Berthoumieux[7], B. Blank[12], C. Borcea[8], A. Cassimi[13], J.M. Daugas[9,1], G. de France[1], F. Dembinski[1], C.E. Demonchy[1], Z. Dlouhy[6], P. Dolégiéviez[1], C. Donzaud[5], G. Georgiev[1], L. Giot[1], S. Grévy[3], D. Guillemaud Mueller[5], V. Lapoux[7], E. Liénard[3], M.J. Lopez Jimenez[1,9], K. Markenroth[14], I. Matea[1], W. Mittig[1], F. Negoita[8], G. Neyens[2], N. Orr[3], F. Pougheon[5], P. Roussel Chomaz[1], M.G. Saint Laurent[1], F. Sarazin[1,10], H. Savajols[1], M. Sawicka[1,11], O. Sorlin[5], M. Stanoiu[1], C. Stodel[1], G. Thiamova[6], D. Verney[1], and A.C.C. Villari[1]

[1] Grand Accélérateur National d'Ions Lourds, B.P. 5027, F-14076 Caen Cedex, France
[2] Instituut voor Kern- en Stralingsfysica, University of Leuven, Celestijnenlaan 200 D, B-3001 Leuven, Belgium
[3] Laboratoire de Physique Corpusculaire, IN2P3-CNRS, ISMRA et Université de Caen, F-14050 Caen, France
[4] Centre de Recherches du Cyclotron, UCL, 2 chemin du cyclotron, B-1348 Louvain-la-Neuve, Belgium
[5] Institut de Physique Nucléaire, IN2P3-CNRS, F-91406 Orsay, France
[6] Nuclear Physics Institute ASCR, CZ-25068 Rez, Czech Republic
[7] CEA Saclay, DSM/DAPNIA/SPHN, F-91191 Gif-sur-Yvette, France
[8] Institute of Atomic Physics, P.O. Box MG6, Bucharest-Margurele, Romania
[9] CEA/DIF/DPTA/PN, BP 12, 91680 Bruyères le Châtel, France
[10] TRIUMF, 4004 Wesbrook Mall, Vancouver, British Columbia, V6T 2A3, Canada
[11] Institute of Experimental Physics, University of Warsaw, PL-00-681 Warsaw, Hoza 69, Poland
[12] Centre d'Etudes Nucléaires de Bordeaux-Gradignan, Le Haut-Vigneau, B.P. 120, F-33175 Gradignan Cedex, France
[13] CIRIL, Rue Claude Bloch, BP 5133, F14070 Caen.
[14] Experimentell fysik, Chalmers Tekniska Högskola och Göteborgs Universitet, S-412 96 Göteborg, Sweden

Received: date / Revised version: date

Abstract. The excitation function for the elastic scattering reaction p(^{18}Ne,p)^{18}Ne was measured with the first radioactive beam from the SPIRAL facility at the GANIL laboratory and with a dedicated solid cryogenic hydrogen target. Several broad resonances have been observed, corresponding to new excited states in the unbound nucleus ^{19}Na. In addition, two-proton emission events have been identified and are discussed.

PACS. PACS-key discribing text of that key – PACS-key discribing text of that key

1 Introduction

Sodium isotopes have been produced in a wide range of the neutron number, from the most neutron-rich isotope ^{37}Na (N = 26) identified for the first time in recent experiments performed at GANIL [1] with the new facility LISE 2000 and at RIKEN [2], to the most neutron-deficient isotope (N=7) lying two steps beyond the proton drip line ^{18}Na [3].

Our knowledge about the ^{19}Na isotope is very limited. The first observation of ^{19}Na was performed in 1969 by Cerny et al. [4] via the transfer reaction ^{24}Mg(p,^{6}He)^{19}Na. The differential cross section for this reaction was about 100 nb/sr in the laboratory frame and the resolution was about 200 keV. They observed one peak at the mass excess of 12.974 ± 0.070 MeV, a value quite close to the value E = 12.90 MeV predicted with the Isobaric Mass Multiplet Equation (IMME). This value of the mass implies this nucleus is unbound against one proton emission. In another experiment, Benenson et al. [5] used the transfer reaction ^{24}Mg(^{3}He,^{8}Li)^{19}Na to study this nucleus. Compared to the previous reaction the differential cross section was about 3 times higher and the energy resolution was about 40 keV. Two peaks were observed and attributed to the ground and first excited states. A more precise value for the mass of the ground state has been measured, which is only E_R = 320 ± 12 keV above the proton emission threshold. The first excited state has been measured at E_x = 120 ± 10 keV above the ground state, but it was observed as a small peak in the tail of the ground-state peak. This result is consistent with the known properties of the other members of the T = 3/2 isobaric analog states multiplet [6], where the first excited state always lies very close to the ground state: in ^{19}O the energy difference is 96 keV, in ^{19}F it is 121 keV and in ^{19}Ne it is 85 keV. In another experiment performed at GANIL and based on the

invariant mass method, Zerguerras et al. [3] were able to measure the mass spectrum corresponding to ^{19}Na. They could see only one peak, at the position of $E_R = 480 \pm 50$ keV. Regrettably, in all these published measurements the intensity for the feeding of the different states was never discussed. It is even very surprising that none of the other excited states was ever observed.

Recently, the second excited state was seen in a precise resonant elastic scattering measurement performed by Angulo et al. [7]. In this case a ^{18}Ne beam impinged onto a thin (0.5 mg/cm^2) polyethylene target. The new state was observed at $E_R = 1066 \pm 2$ keV, with a width of $\Gamma = 101 \pm 3$ keV and a spin of $J^\pi = \frac{1}{2}^+$. This state corresponds undoubtedly to the known second excited state in the mirror nucleus ^{19}O. It is 725 keV down shifted from its analog.

We report here the results of a new study. We have measured the resonant elastic scattering of a ^{18}Ne beam onto a thick solid cryogenic hydrogen target. This experiment was the first experiment performed with a radioactive beam from the SPIRAL facility at GANIL. In the following sections 2-5 we present the experimental conditions of this measurement. The analysis of the excitation function is presented in the sections 6-8. It is also presented several calculations, using a potential model and the shell model, to compare with the measured properties and with the known states in the mirror nucleus ^{19}O. In the final sections 9-10 two-proton events observed in the same experiment are analyzed and discussed.

2 Principle of the measurement

In order to investigate the structure of the ^{19}Na isotope, we have measured the excitation function of the elastic scattering reaction ^{18}Ne(p,p)^{18}Ne. The experimental excitation function for the elastic scattering at low energy can mainly be described by the Rutherford elastic scattering formula, but it also shows up "anomalies", i.e. various kinds of resonances that are related to discrete states in the compound nucleus. The excitation energy of the states can be determined from the position of the resonances, the partial widths of the states from the width and intensity of the resonances, and the spin and parity of the states from the shape of the resonances and the angular distributions. This measurement is simple, it gives pertinent properties of the states, and the cross sections are often high, an essential condition when dealing with radioactive nuclei.

As ^{18}Ne is radioactive ($T_{1/2} = 1.672$ s), we have measured this elastic scattering in inverse kinematics: p (^{18}Ne,p) ^{18}Ne. Consequently, the experiment benefits of two important effects: a focusing effect that allow to increase the counting rate by a factor of about 4 for a forward angle detector, and an energy effect that improves the reconstructed resolution in the center of mass frame by a factor of close to 4 in comparison to the resolution measured in the laboratory frame.

It is very time consuming, specially using relatively low intensity radioactive beams, to change the energy of the incoming beam by small steps to measure the full excitation function. To solve this problem we can use a thick target. The idea of using a thick target has been developed successfully in several experiments [8–10]. If the energy of the impinging particle (^{18}Ne), at some point along its slowing down trajectory inside the target, corresponds to an excited state of the compound nucleus (^{19}Na = ^{18}Ne + p), the probability for elastic scattering changes significantly. The scattered proton can escape the target because of its smaller energy loss, and can be detected at forward angles in the laboratory frame after escaping the target. There is a direct correspondence between the energy of the detected proton and the center of mass energy of the scattering event. In our experiment the target was thick enough to stop the beam inside the target. Therefore, the thick target makes it possible to obtain a complete and continuous excitation function over a wide range of energies, by simply detecting the scattered protons and measuring their energies, without changing the energy of the incident beam. As measured for example by Axelsson et al. [8] with a thick target, the final resolution can be better than 50 keV in the center of mass frame, generally good enough to study states with large widths. The disadvantages to use a thick target are discussed hereafter.

3 Experimental setting

The elastic scattering measurement has been performed at GANIL with a radioactive beam produced by the new SPIRAL (Système de Production d'Ions RAdioactifs en Ligne) facility [11,12]. The ^{18}Ne beam has been produced through the projectile fragmentation of ^{20}Ne primary beam at 95 A MeV on a carbon target, located at the new underground production cave of SPIRAL. For this first experiment, a maximum primary beam intensity of ~ 0.20 pμA has been used, in order to limit the irradiation of the production ensemble. The radioactive atoms released from the carbon target - heated at 2000 K - were ionized by the compact and totally permanent magnet Nanogan-3 ECR ion source to the charge state 4+. The beam was accelerated by the new compact cyclotron CIME (Cyclotron d'Ions à Moyenne Energie) up to an energy of 7.2 A MeV. The beam was contaminated by 15 % of ^{18}O and a very small amount ($< 1\%$) of ^{18}F. The efficiency of the overall production system can be disentangled in the following way: More than 90% of the produced atoms diffuse out of the target and arrive in the ECR ion source. About 15% of these atoms are extracted in the charge state 4+. The transmission of the low energy separator, corresponding to the first half of the injection line of CIME was of the order of 50%, while the transmission of the CIME accelerator including the beam pulsing and beam extraction was also 50%. The observed efficiencies were compatible with those expected. The present design of the Carbon target allows to increase of the primary beam intensity up to 1 pμA, which will correspond to 10^7 particles per second of ^{18}Ne. It should be pointed out the excellent stability and reproducibility of the whole production and acceleration

system of SPIRAL. During the experiment one could easily change the tuning of the cyclotron from ^{18}O, used for calibrations, to ^{18}Ne in about 15 minutes. To get rid of the contamination we have used the LISE magnetic spectrometer as a separator. A thin carbon stripper foil (40 μg/cm^2) was placed at the target position of the spectrometer to select the 10+ charge state of the beam, yielding a pure $^{18}Ne^{10+}$ beam with a mean intensity of 2.5 10^5 pps. All along this experiment, the beam intensity was measured and monitored by using a multi channel plate detector placed in front of the target.

We have chosen to use a solid cryogenic hydrogen target of 1 mm. We have used a pure hydrogen target for two reasons. First, the use of compound targets (e.g. $(CH_2)_n$) introduces other elements (e.g. Carbon) in which new reactions can occur and may pollute the measurement. We have performed several tests with this kind of target and we have observed that the carbon contributes as a non negligible continuous background at our incident energy. Second, the use of a pure hydrogen target maximizes the counting rate because the highest stoechiometric ratio leads to the highest effective target thickness. The main requirements imposed for the development of solid cryogenic targets usable under vacuum are: low thickness, very thin windows, and uniform thickness and density. A special cryogenic system has been designed to make this target [13]. Cryogenic target systems have already been designed in various laboratories, particularly by directly condensing H_2 gas to make the target. In the system developed at GANIL, we have opted for a transition to the liquid phase (16.2 K - 230 mbar) before progressive solidification of the hydrogen (T < 13.9K) [14]. Liquid helium has been used as a cold source at 4 K and the growth of the crystal has been imposed by the temperature gradient in the metal frame supporting the target. The target has been made using a metal frame to which mylar windows were glued. A stack of frames has formed an H_2 target cell with an He cell on either side of the target. During the target production phase, equivalent pressure has been maintained on either side of the target windows. Once the target was formed, the helium gas was evacuated. The density of the target was probably not perfectly constant over its entire length (expected 0.8 % variations). We have used a 1 mm thick target and 6 μm mylar windows. The diameter of the entrance windows was 10 mm. The time required to produce the solid target, after placing the cryostat under vacuum, was about 3 hours and the system consumed $\sim$ 1 liter/h of liquid helium to maintain the solid target at low temperature (depending on the quality of vacuum). The target has been placed in the experiment vessel to intercept the beam during nearly a week (P $\sim$ 20 μW on the target) and during all the experiment the target temperature has stayed below 9K.

In our experiment the scattered protons escaped from the cryogenic target and were detected in a telescope of silicon detectors. The telescope was composed of 3 silicon detectors, 50 x 50 mm sized: a 150 μm ΔE detector, an 1 mm double-sided strip detector and a thick 3.5 mm Si(Li) detector. The large total thickness of the telescope has been chosen in order to cover a large proton energy interval. The ΔE detector was placed 317 mm behind the target in order to decrease the counting rate due to the β rays from the decay of the beam particles. The second silicon detector was placed just behind the first one. The angular acceptance was $d\Theta^1_{lab} = \pm\ 4.5°$ in the laboratory frame, corresponding to a solid angle of $d\Omega^1_{lab} = 20$ msr. Due to geometrical constraints the Si(Li) detector was placed farther away from this ensemble, 495 mm from the target, corresponding to a relatively narrower angular acceptance of $d\Theta^2_{lab} = \pm\ 3°$ and to a solid angle of $d\Omega^2_{lab} = 10$ msr. Moreover, during a part of the experiment we have used an other configuration in which the second detector was removed.

4 Test and Calibration with p(^{18}O,p)^{18}O

From the raw spectra, several corrections must be applied to obtain the excitation function. A first correction (figure 1-a) is applied for the energy loss of the protons inside the hydrogen target. Simulations have been performed with the energy losses calculated with the program SRIM [15]. We can observe that the energy loss changes very slowly (maximum difference of 150 keV) over the full range of the proton energies we are interested in (between 2.5 MeV and 25 MeV in the laboratory frame).

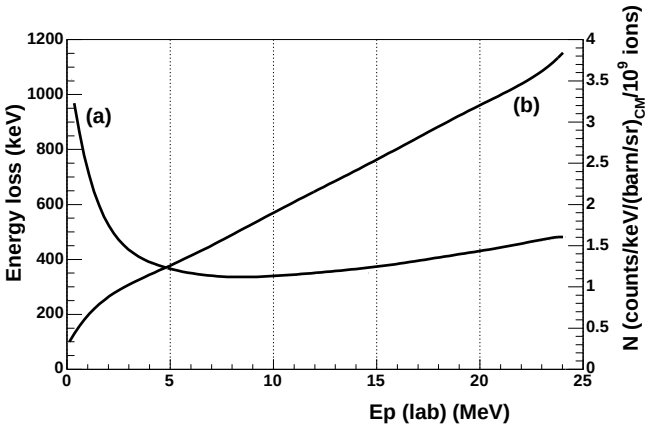

Fig. 1. Results from one simulation of our experiment with an ^{18}O incident beam. (a): Left axis. The energy loss (in keV) of the protons inside the hydrogen target is plotted versus the detected proton energy (in MeV) in the laboratory frame. (b): Right axis. The number of counts N (per (barns per steradian) in center of mass frame, per 10^9 incident ions, per keV in laboratory frame) is plotted as a function of the detected proton energy.

The second correction (figure 1-b) has to be applied for normalization. The effective target thickness at a certain energy depends on the energy loss of the incident ions at this energy. This effect explains why it is very important to use a pure hydrogen target. In that case, we obtain the

lowest energy loss and the highest proton density, which both increase the counting rate. Another part of the dependance is also coming from kinematical effects. We can observe that the counting rate (per (barns per steradian) in center of mass frame, per 10^9 incident ions, per keV in laboratory frame) increases with energy. We are more sensitive to higher energies, which compensates for the usually lower cross section at those energies.

The simulations have also shown that the energy resolution is a soft function of the center of mass energy. With a ^{18}Ne beam, the energy straggling goes from $\sigma_{lab} = 37$ keV at the highest detected energies up to $\sigma_{lab} = 41$ keV at the detected energy of 2.5 MeV. Taking into account the detector resolution and the energy uncertainty coming from the angular acceptance of the detector, we calculated a total center of mass frame resolution of $\sigma_{cm} = 25$ keV, a value that underestimates the real one because of the experimental non uniformity of the target thickness.

We performed a measurement with a stable beam for several reasons: to determine the mean target thickness, to evaluate the thickness uniformity of the cryogenic target, to test the analysis program. This measurement was accomplished with an ^{18}O beam, produced at the same energy as ^{18}Ne. The energy of the incident beam (7.2 A MeV) has been chosen to stop the ^{18}O beam at the downstream edge of the target. The final result is shown in figure 2. This spectrum has been measured in 2.8 hours, with a mean beam intensity of 10^6 pps.

From our measurement we were able to perform two comparisons:

- A part of our measured excitation function was already measured in direct kinematic by Orihara et al. [16] in a very precise experiment ($\sigma_{lab} \sim 2.5$ keV). The related data are shown in the insert of figure 2 as a dotted line. The measured angle in this reference $\Theta_{CM} = 168.7$ ° is not equal to our mean value $\Theta_{CM} = 180$ °, but it is close enough to make that comparison interesting. The comparison shows a good agreement in energy and in normalization. Through the comparison, used as a calibration measurement, it was possible to determine precisely the mean target thickness $\bar{d} = 1050 \pm 20$ μm (constant density of 88.5 mg/cm^3). Moreover, we found an energy resolution of $\sigma_{CM} = 30 \pm 10$ keV, constant in this range of energy. This value is in good agreement with those obtained in similar experiments [8] using homogenous gas targets. Using this value of the energy resolution, we have determined a target thickness uniformity of $\sigma_{target} = 70$ μm, demonstrating the good quality of the cryogenic system used here. Furthermore, a small correction in normalization has led to the corrected value for the solid angle of $d\Omega_{lab} = 11 \pm 1$ msr (configuration using the Si(Li) detector).
- The properties of the ^{19}F (^{18}O + p) states lying at excitation energies $8 \leq E_x \leq 15$ MeV are quite well-known. We have compared our measurement with a R-matrix calculation performed using 37 known states (from [16,6]) of ^{19}F. These states corresponds to all known states in the measured energy range. The R-matrix calculation has been performed with the code Anarki [17]. Figure 2 shows the result of this calculation as a continuous curve, performed at the angle of $\Theta_{CM} = 180$ ° and using the same energy resolution as the experimental one. Again we can observe an overall excellent agreement, in normalization and in energy. Moreover, no extra peak is visible in the spectrum. However, the agreement between the calculation and our measurement is not perfect, we can observe differences, mainly in normalization. We have observed negligible differences in the calculations when angles are chosen within the angular acceptance of the detectors. In fact, the differences are mainly due to the uncertainties in the known properties of the excited states in ^{19}F. For example, we don't know precisely the width for all excited states in that nucleus. The low energy part of the spectrum was calibrated in energy using the results of the R-matrix calculation. In figure 2, at $E_{gap}^{CM} \approx 1.1$ MeV there is an energy-gap of ≈ 200 keV with no data. This gap results from dead layers between the first ΔE detector and the next one, and selection conditions. The protons with energies higher than this energy gap are identified and selected using a standard contour in a ΔE-E plot. The lower energy part of the spectrum is produced by a different technique. Firstly, we have applied a time of flight selection to identify the protons. Secondly, to select the particles stopped in the first detector we applied a low energy threshold on the second detector.

In conclusion, this calibration measurement allowed us to extract different parameters of our experimental setting (calibration, target thickness, resolution etc.), and the values for those parameters were very close to those expected.

5 Measurement of p(^{18}Ne,p)^{18}Ne

In the case of the radioactive ^{18}Ne beam, the same analysis of the data as described in the previous paragraph has been applied to produce the ^{19}Na spectrum of figure 3. It represents a 38 hour measurement. For the analysis we have used exactly the measured values of the experimental parameters deduced from the ^{18}O calibration measurement. The unique difference is in the energy resolution. Indeed, since ^{18}Ne does not stop at the same position (430 μm from the target edge instead of 70 μm), the energy resolution in the center of mass frame is calculated to be 2 keV worse for ^{18}Ne than for ^{18}O.

From a comparison with figure 2, we can clearly observe similarities, several resonances are present, but with also some differences, in particular there are much less resonances observed (labelled from A to F), and they all have large widths. Indeed, the compound nucleus ^{19}Na is populated at low excitation energies which correspond to a region of a lower density of states.

6 Analysis and discussion

We have performed a similar R-matrix analysis to that performed in the case of ^{18}O+p. For the first peak la-

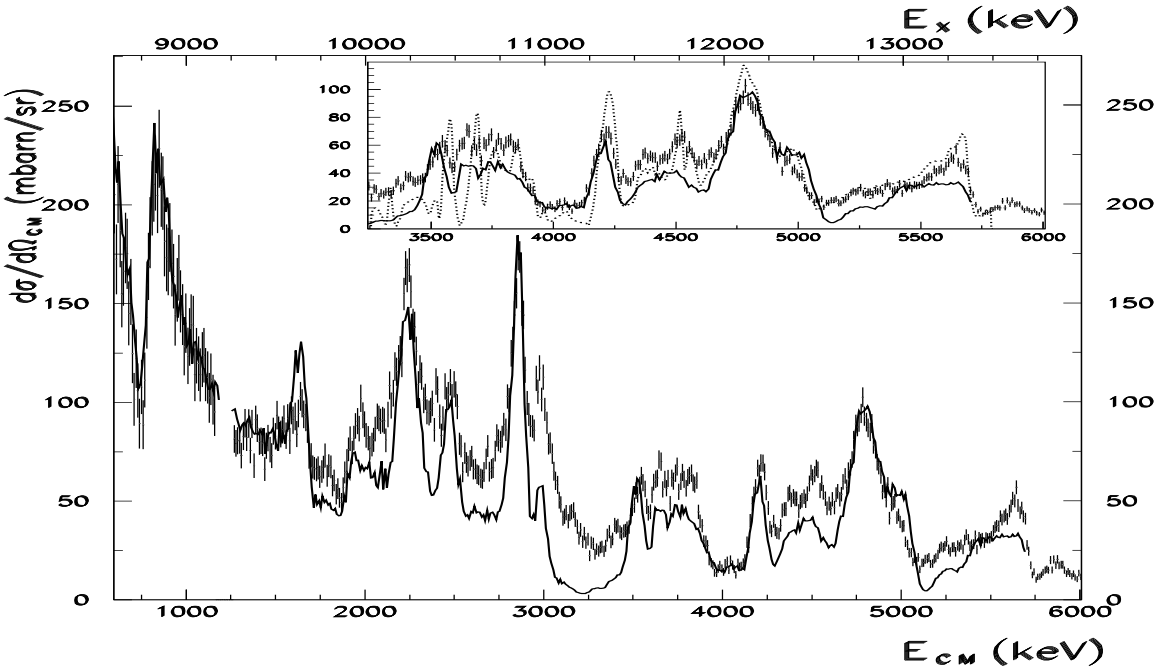

Fig. 2. The measured excitation function for the elastic scattering reaction ^{18}O(p,p)^{18}O. The reconstructed differential cross section (CM, $\Theta = 180°$) is plotted as a function of the center of mass energy E_{CM} (lower axis) and the excitation energy E_X in ^{19}F (upper axis). The error bars are statistical. The continuous curve represents a R-Matrix calculation using the known properties of states in ^{19}F. All widths are not known, this may explain the differences between the experimental data and the calculated excitation function. The experimental resolution is measured to be $\sigma = 30$ keV. Insert: a zoom of the high energy part of the spectrum is shown, the continuous curve corresponds to the R-Matrix calculation, the dotted curve represents the data from Orihara et al. [16].

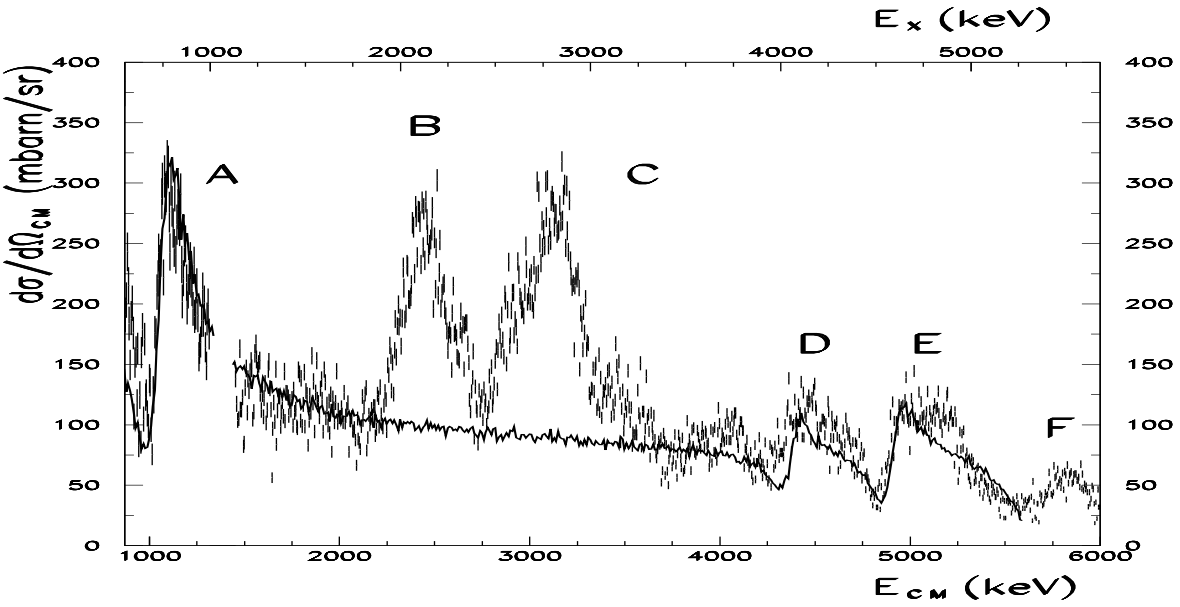

Fig. 3. The reconstructed differential cross section (CM, $\Theta = 180°$) for the elastic scattering reaction ^{18}Ne(p,p)^{18}Ne is shown as a function of the center of mass energy E_{CM} (lower axis) and the excitation energy E_X in ^{19}Na (upper axis). The labels correspond to the peaks described in the text. The continuous line represents a R-Matrix calculation when the properties of four states of ^{19}Na are taken into account (see text).

belled A in figure 3, the characteristic shape of the peak corresponds to a $J^\pi = \frac{1}{2}^+$ assignment. For that state we obtained $E_{CM} = 1076 \pm 6$ keV and $\Gamma = 80 \pm 20$ keV. These values are in good agreement with the already known properties of the second excited state in ^{19}Na, previously measured at $E_{CM} = 1066 \pm 2$ keV with a width of $\Gamma = 101 \pm 3$ keV [7]. Taking into account the two results we obtain a mean value of $E_{CM} = 1067.0 \pm 1.9$ keV and $\Gamma = 100.5 \pm 3.0$ keV. It is very interesting to compare this level with the known levels in ^{19}O, since the position of the excited states and the spectroscopic factors should be nearly identical for mirror nuclei. The level is at an excitation energy of $E_x = 747 \pm 14$ keV in ^{19}Na, which only matches in the mirror nucleus with the known $\frac{1}{2}^+$ state at a position of $E_x = 1471.7 \pm 0.4$ keV. This means that the corresponding state in ^{19}Na has been down shifted by $\Delta = 725$ keV $\pm$ 15 keV. To study the energy shift due to the Coulomb interaction we have performed calculations using a potential model. In a first step, we have fitted the depth of a Wood-Saxon well to reproduce the position of the analog state in ^{19}O. The state is calculated with a model of one neutron in the potential of a ^{18}O core. In a second step we have computed the isospin symmetric system of one proton in the potential of a ^{18}Ne core. For that calculation we have used the same nuclear potential as fitted in ^{19}O, in addition to the Coulomb interaction for the proton. The calculation shows an energy shift between analog states. The largest correction is observed for the s-orbital, which corresponds to the $J^\pi = \frac{1}{2}^+$ assignment of the state. In that case, the energy shift is calculated to be $\Delta = 749$ keV, a value very close to the experimental one. This kind of calculation is clearly a good approximation when the studied states can be well described by the simple model of one particle plus a core, i.e. when the spectroscopic factor ($\theta^2_{s.f.}$) for this configuration is close to 1. This is exactly the case in the mirror nucleus, the analog state is known with a measured value $\theta^2_{s.f.} = 1$. We performed a shell model calculation for that state, and it predicts a value very close to one, $\theta^2_{s.f.} = 0.83$. This calculated value of the spectroscopic factor, using our simple potential model, is equivalent to a width of $\Gamma = 96$ keV, again in agreement with the experimental value. In conclusion, this state can be mainly described by the shell model configuration $\pi(1d5/2)^2(2s1/2)^1$.

The peak labelled B is intense and broad, with $\Gamma \approx 300$ keV, and is positioned at an energy $E_{CM} \approx 2.4$ MeV corresponding to an excitation energy $E_x \approx 2.1$ MeV. Surprisingly it does not match any known state at the same position in the mirror nucleus. There are two known states in ^{19}O at energies of $E_x = 2.3715$ MeV and $E_x = 2.7790$ MeV, but they can not match because they are assigned with spins $J^\pi = \frac{9}{2}^+$ and $\frac{7}{2}^+$, both corresponding to angular momentum number $\ell = 4$, which is excluded in our experiment because of the expected very narrow width for such a high angular momentum barrier. There are also two other known states in the mirror nucleus, positioned at excitation energies of $E_x = 3.0671$ MeV and $E_x = 3.1535$ MeV, with spin $\frac{3}{2}^+$ and $\frac{5}{2}^+$, corresponding to an angular momentum number $\ell = 2$, but they also can not match because the Coulomb energy shift can not be so large as to explain the difference in energy.

The peak labelled C, positioned at an energy of $E_{CM} \approx 3.1$ MeV, corresponding to an excitation energy of $E_x \approx 2.8$ MeV, has a width of $\Gamma \approx 500$ keV. The intensity and the shape of the peak are very similar to those of the peak B. We have performed R-matrix calculations to simulate the elastic scattering including that state. In no case the calculations have fitted the experimental results.

In order to understand the origin of the peaks B and C, we have performed shell-model calculations. There are two main objectives for these calculations:

- All states are certainly not known experimentally in the mirror partner ^{19}O. Performing shell-model calculations gives the possibility to predict the positions of states in ^{19}Na.
- Calculations give the possibility to predict the spectroscopic factors $\theta^2_{s.f.}$, i.e. the superposition probabilities between the entrance channel ^{18}Ne + p and the different states in the compound nucleus ^{19}Na*, and also between the different states in ^{19}Na* and the different inelastic scattering channels ^{18}Ne* + p, which finally allow the calculation of the widths for elastic and inelastic scattering.

For the nuclei with A = 19 and T = 3/2 we have performed a shell-model calculation in the spsdpf space and with the WBT [18] interaction. This calculation has been carried out with the shell-model code Oxbash [19]. We have allowed 0 and 1 $\hbar\omega$ excitations, which have permitted the rising of low-lying negative-parity states. We have calculated all states up to $E_x = 5.5$ MeV, and all elastic scattering channels up to the angular momentum number of $\ell = 3$. We have also calculated all inelastic scattering channels on the first excited state in ^{18}Ne (2^+, $E_x = 1887$ keV [6]). We have used the experimental values of the excitation energies E_x^{exp} (see table 1) for the states in ^{19}Na or those known in the mirror nucleus. The partial widths are estimated in the standard way from the expression $\Gamma = 2\theta^2_{s.f.}\gamma^2 P(\ell,Q)$ where Q is the particle-decay energy, γ^2 is the Wigner single-particle width and $P(\ell,Q)$ is the penetrability, l is the angular momentum of the transition. The penetrabilities are calculated in a Woods-Saxon well using the correct number of nodes of the wave functions. The summary of the calculations is given in table 1. It is interesting to notice that no state corresponding to the position of the peaks B and C is present in the table. A $\frac{1}{2}^-$ state (labelled 4) is positioned at $E_x = 2405$ keV, but with a too narrow width of 6.1 keV to explain them. The state labelled 5 is positioned close to the position of the peak C. However, the predicted width is much too narrow to match. In fact, after a careful analysis we conclude that the peaks B and C have a shape and an intensity that can not match any interpretation in the frame of the simple elastic scattering.

To study the peaks D and E of figure 3 we proceeded an iterative analysis. The first two states in ^{19}Na (1 and 2 of table 1) are predicted to be too narrow to be observed. The known properties of state labelled 3 in table 1 have

Table 1. Predicted properties of states in ^{19}Na from shell model calculations. We used Q_p = -320 keV. The symbol E_x^{exp} corresponds to the values we have used to calculate the widths Γ_{gs} and Γ_{2^+}, they correspond to the measured values of the excitation energies when known [5,7], or the excitation energies measured in the mirror nucleus ^{19}O [6]. When it is not known, the predicted values E_x are used.

Label	J^π	E_x (keV)	E_x^{exp} (keV)	Γ_{gs} (keV)	Γ_{2^+} (keV)
1	$\frac{5}{2}^+$	0	0	0.2 eV	-
2	$\frac{3}{2}^+$	293	120	0.6 eV	-
3	$\frac{1}{2}^+$	1467	746	86	-
4	$\frac{1}{2}^-$	2405	-	6.1	4 eV
5	$\frac{5}{2}^+$	3167	3153	5.4	367
6	$\frac{3}{2}^+$	3746	3231	2.4	203
7	$\frac{3}{2}^-$	4258	3944	51	17 eV
8	$\frac{5}{2}^-$	4667	4582	45	80 eV
9	$\frac{1}{2}^-$	4890	-	0.1	29
10	$\frac{5}{2}^+$	5010	-	6.9	216
11	$\frac{3}{2}^-$	5466	-	161	1.3

been introduced into the R-matrix program to produce a first excitation function, which fitted well the peak A using the slightly different values of width and energy reported in the table 2.

Table 2. Properties of the peaks measured in ^{19}Na when figure 3 is interpreted as a pure elastic scattering. However, our R-matrix calculations can not fit the peaks B and C, the values are just indicative. See figure 3 and table 1 for labels.

Labels	J^π	E_x (keV)	Γ_{gs} (keV)
A - 3	$\frac{1}{2}^+$	756 ± 6	80 ± 20
B	-	≈ 2.1 MeV	≈ 300 keV
C	-	≈ 2.8 MeV	≈ 500 keV
D - 7	$\frac{3}{2}^-$	4371 ± 10	30 ± 10
E - 8	$\frac{3}{2}^-$	4903 ± 10	50 ± 10

In a second step we introduced in the R-matrix program the states predicted with $\Gamma_{gs} > 10$ keV, i.e. the three states labelled 7, 8 and 11 of table 1. They all have spin $\frac{3}{2}^-$. Starting from the predicted properties for these states, we have computed an excitation function which was in a good agreement with the experimental excitation function. It reproduced the peaks D and E when we used the slightly modified properties reported in table 2. The predicted properties for the state 11 have been used without modification, but can not be used as real measured properties since states at excitation energies higher than 5 MeV are difficult to analyze. Indeed, at these high energies there is a quite high density of broad states which are not easy to disentangle.

The final result of the above analysis is plotted in figure 3 as a continuous line. We can observed an good overall agreement, except for the peaks B and C.

7 Inelastic scattering

The two main observed peaks B and C can not be explained by the elastic scattering channel. Nevertheless, the shell-model calculations (table 1) have revealed several states with broad widths in the inelastic channel, corresponding to the reaction: p(^{18}Ne,p)^{18}Ne*(2^+,1.887 MeV). The use of a thick target does not allow us to separate the different contributions, this is the main disadvantage of using a very thick target, the inelastic scattering contribution is added to the elastic scattering. The question then arises whether the two peaks could be explained by inelastic scattering process. The observed shape of the peaks may fit with what is expected from an inelastic scattering. But the inelastic scattering cross sections is usually at least a factor 10 times lower than the elastic scattering cross sections. However, in the hypothesis of an inelastic scattering contribution, the excitation function has to be re-analyzed to take into account other kinematics and energy losses. This may affect drastically the excitation function. The re-analysis of the data has been performed in several steps. First, we have subtracted the calculated excitation function of figure 3 from the experimental excitation function to reveal the hypothetical inelastic contribution. Then we have re-analyzed this spectrum to produce an excitation function. It resulted in the final experimental histogram shown in figure 4.

We can observe that peaks B and C are at energies close to the predicted positions for states 5 and 6 (from table 1). A calculation has been performed with the program Anarki to predict the excitation function for the inelastic scattering. We tried for states 5 and 6 different values of the parameters. A typical result is shown in figure 4 (using $\Gamma_{gs} = 10$ keV and $\Gamma_{2^+} = 200$ keV) as a filled surface (amplified by a factor 5). We can observe that the agreement is good for the shape and the position of the peaks, but there is a very large discrepancy in the intensity. Only a small part of the experimental peaks may be due to the inelastic scattering contribution. Our conclusion is that the two main peaks B and C can not be explained only by the elastic neither the inelastic scattering channel. Therefore, we have searched for other possible processes.

8 Two-proton emission from ^{19}Na

At our incident energy, several reaction channels are open:

– In the case of ^{18}O: ^{18}O + p (elastic scattering), ^{18}O* + p (inelastic scattering with gamma emission), ^{15}N + α (Q = +3.98 MeV), ^{16}O + ^{3}H (Q = -3.7 MeV), ^{18}F + n (Q = -2.44 MeV), ^{17}O + d (Q = -5.82 MeV), ^{14}N + n + α (Q = -6.85 MeV), ^{14}C + p + α (Q = -6.23 MeV).

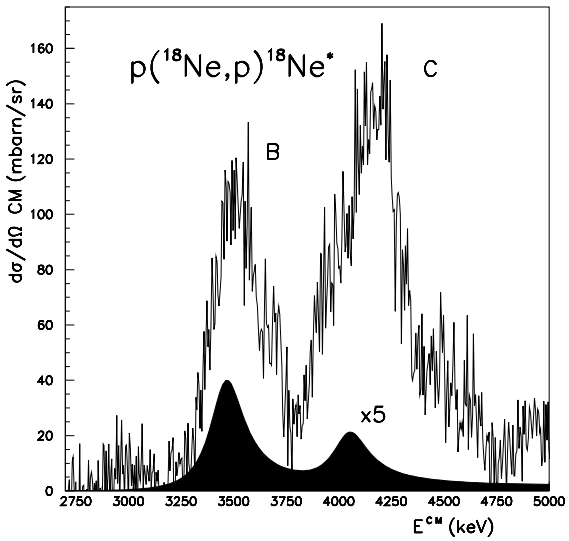

Fig. 4. Peaks B and C from figure 3 have been re-analyzed in the inelastic scattering hypothesis. This new result is compared with a R-matrix calculation (the black surface amplified by a factor 5) using peaks 5 and 6 from table 1 with $\Gamma_{gs} = 10$ keV and $\Gamma_{2^+} = 200$ keV. Although the shape and the position of the peaks are in good agreement, the intensities are very different.

– In the case of ^{18}Ne: ^{18}Ne + p (elastic scattering), ^{18}Ne* + p (inelastic scattering with gamma emission), ^{17}F + 2p (Q = -3.922 MeV), ^{16}O + 3p (Q = -4.522 MeV), ^{14}O + α + p (Q = -5.113 MeV).

Several of these inelastic reactions result in the emission of protons, which might produce extra peaks in our excitation function. Therefore, it is important to measure the contribution of these different channels. For that objective we examined several questions:

– Do we feed other reaction channels than the elastic scattering ? To answer this question we used a telescope of silicon detectors. The telescope has allowed a clear identification of the particles with a standard E-ΔE plot. We have identified several channels, mainly β radioactivity rays or α particles production, but the telescope allowed the rejection of those particles. The α particles are observed as a low intensity contribution and with a continuous energy distribution, in contrast with the proton distribution.
– Do we have several contributions in the proton spectra ? We have performed several experimental tests with stable beams (^{18}O, ^{12}C, ^{24}Mg) to answer that question. The very good agreement found in the analysis of the data for the ^{18}O beam is in agreement with the hypothesis that other channels are negligible. Moreover, no extra peak was visible in the ^{18}O excitation function, even if several reaction channels are open including those with proton emission. In conclusion, in the case of stable beams there was no other contribution in the excitation function.
– Is the previous conclusion still valid for the ^{18}Ne radioactive beam ? In order to clarify this point an additional analysis was performed with a silicon strip-detector, allowing the detection of particles in coincidence. In the case of the ^{18}O beam, no coincidence event was observed. But, in the case of the ^{18}Ne beam, we observed events with proton multiplicity equal to 2.

We have observed a few hundred of events with two protons detected in coincidence. Thus, the spectrum corresponding to the detection of single protons should be contaminated by protons coming from two-proton emissions. Indeed, the probability to detect only one proton after a two-proton emission is much larger than the probability to detect the two protons in coincidence. In fact, in that case the probability is larger by a factor $\Re$, which depends on the angular distribution of the two protons and the solid angle of the detectors.

In figure 5, we plotted the individual laboratory energies from two-proton events (continuous line) and compared it with the energies in laboratory obtained in the region of the peaks B and C (elastic scattering background subtracted) when only one proton is detected (dashed line).

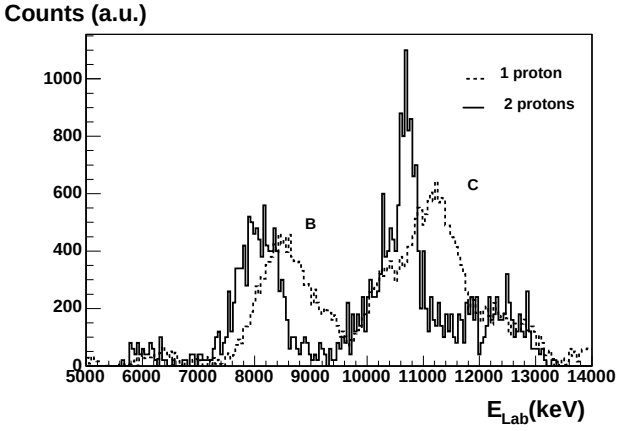

Fig. 5. The individual energies in laboratory frame of the two-proton events (continuous line) are plotted and compared with the energies obtained when only one proton is detected (dashed line). A similar pattern is observed in the region of the peak B and C.

A similar pattern is observed for the two plots, two peaks are present but shifted in energy. These observed differences may be due to kinematical effects. Indeed, when we have two protons emitted from a nucleus, the second proton is shifted due to the emission of the first one. This effect has been estimated from a simulation using a sequential emission process and an uniform angular distribution in center of mass. We found that kinematics produce an energy shift in agreement with the observed one. Moreover, the factor $\Re$, corresponding to the ratio between

the number of one-proton events divided by the number of two-proton events, has been estimated from our simulation, and has been found to be $\Re^{sim} = 67$, close to the experimental value $\Re^{exp} = 83$, which corresponds to the ratio between the number of protons in the two peaks B and C divided by the number of detected two-proton events.

Thus, our conclusion is that the two peaks labelled B and C result from a complex combination of several two-proton emissions but when only one of the two protons is detected.

9 Analysis of the two-proton events

The analysis of the two-proton events can be performed in the framework of a sequential mode, i.e. the 2 protons are emitted one after another from one initial state in the compound nucleus ^{19}Na, through one intermediate state in the nucleus ^{18}Ne. But that problem has an infinite number of solutions because we start with the two measured energies (e1 and e2) for the transitions and we have to deduce 3 excitation energies: the initial state in ^{19}Na, the intermediate state in ^{18}Ne, and the final state in ^{17}F. To obtain a solution we have to assign the final state of ^{17}F in the initial conditions. However this problem still gives two solutions, because we do not know which proton has been emitted first. An example of an ensemble of solutions is shown in figure 6 in the case where the final state is the ground state of ^{17}F.

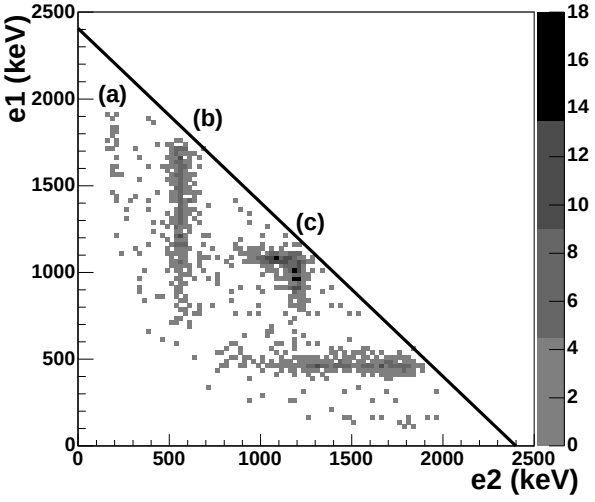

Fig. 6. The reconstructed two dimensional energy distribution of the experimental two-proton events. The y axis corresponds to the center of mass energy of the first transition, from one excited state in ^{19}Na to one excited state in ^{18}Ne, the x axis is the energy of the second transition from the state in ^{18}Ne to $^{17}F_{gs}$. The continuous line corresponds to the maximum energy available in center of mass system. The 3 clusters of events producing the vertical lines labelled (a), (b) and (c), correspond to sequential transitions (see text).

In figure 6 the center of mass energy of the first transition is plotted versus the energy of the second transition. It is very interesting to observe that the points aligned along straight lines, thus providing a hint for a sequential decay. Indeed, the kinematical and energy loss corrections between the detected energies and the center of mass energies are so strong, that this observation constitutes a confirmation of our interpretation of the data. This also means that the final state $^{17}F_{gs}$ is a realistic hypothesis. The widths of the lines correspond to widths of the transitions. The energy resolution of the method has been estimated to be about 40 keV. The final interpretation is chosen after checking two conditions: the maximum energy available in the center of mass is limited by the beam energy, and the first transition has always to be broader than the second one, because the width of the first transition is a convolution of the width of the initial state with the width of the intermediated state. In figure 6 we can observe 3 clusters of points, the vertical lines labelled (a), (b) and (c). The analysis of the data has been performed using the Breit-Wigner formula for the shape of the states. The maximum energy available in the center of mass is indicated by the line $e_1 + e_2 = 2400$ keV in figure 6. We can observe that some events are very close to that limit, this may indicate that some transitions are cut. In the analysis, an energy limit has been introduced to take into account this effect. The total widths Γ_{tot} of the states have been determined taking into account our energy resolution. The results of this analysis are summarized in table 3.

Moreover, the first excited state in ^{17}F is only 495 keV above the ground state. We have also to consider the decay to this final state. In this hypothesis there is not enough energy left in the center of the mass frame to interpret a large part of the events seen in the transitions (b) and (c) of figure 6. This means it is not the correct interpretation for these events. On the other hand, all the events of the transition (a) can be analyzed in that hypothesis. The results are summarized in the last row of table 3 and labelled (a*).

As a final check we have compared our measured states on ^{18}Ne with the known properties of the excited states in that nucleus.

The state determined from transition (a) in the first row of table 3 is not known, the closest states in ^{18}Ne are a 1^- state positioned 399 keV above our measured state, at $E_x = 4520 \pm 7$ keV [20], and a 2^+ state positioned 505 keV below, at $E_x = 3616.4 \pm 0.6$ keV [21]. On the contrary, a correspondence can be found within the error bars in the (a*) hypothesis. There is a known state at $E_x = 4589 \pm 7$ keV, with $J^\pi = 0^+$ [21], which gives +17 keV energy difference. There are two other known states at $E_x = 4523.7 \pm 2.7$ keV, with $J^\pi = 3^+$ [22], and at $E_x = 4520 \pm 7$ keV, with $J^\pi = 1^-$ [21], which give an energy difference of -48.3 keV and -52 keV. Our measured width is also in agreement with the known values $\Gamma = 4 \pm 4$ keV, $\Gamma = 18 \pm 3$ keV and $\Gamma = 9 \pm 6$ keV. In the 0^+ hypothesis, the proton may decay to the ground state of ^{17}F ($J^\pi = \frac{5}{2}^+$) or to the first excited state at $E_x = 495$ keV ($J^\pi = \frac{1}{2}^+$). In the first case, it means the transition

Table 3. Results corresponding to the two-proton events analyzed in the sequential mode. The widths Γ_{e1} and Γ_{e2} refer to the widths of the proton transitions, and Γ_{tot} to the widths of the excited states.

Label	$e_1(^{19}Na \rightarrow ^{18}Ne)$ (keV)	Γ_{e1} (keV)	$E_x(^{19}Na)$ (keV)	$\Gamma_{tot}(^{19}Na)$ (keV)	$e_2(^{18}Ne \rightarrow ^{17}F_{gs})$ (keV)	Γ_{e2} (keV)	$E_x(^{18}Ne)$ (keV)	$\Gamma_{tot}(^{18}Ne)$ (keV)
a	1698 ± 75	541 ± 178	5499 ± 76	539 ± 180	200 ± 12	40 ± 34	4121 ± 12	9^{+54}_{-9}
b	1424 ± 30	697 ± 72	5585 ± 32	695 ± 72	560 ± 11	47 ± 4	4481 ± 11	27^{+6}_{-9}
c	1018 ± 13	154 ± 17	5815 ± 17	141 ± 18	1196 ± 11	51 ± 6	5117 ± 11	33^{+9}_{-11}
					$e_2(^{18}Ne \rightarrow ^{17}F_{p1})$			
a*	1557 ± 66	463 ± 215	5809 ± 76	460 ± 215	156 ± 12	39 ± 15	4572 ± 12	0^{+37}_{-0}

has l = 2 momentum transfer, and for the second case l = 0. The lower angular momentum barrier may explain why we observe the transition to the first excited state.

The state determined from the transition (b) can be associated with two states in ^{18}Ne: the state at $E_x = 4520 \pm 7$ keV, $J^\pi = 1^-$, or the state at $E_x = 4523.7 \pm 2.9$ keV, $J^\pi = 3^+$. In those cases the differences in energy are Δ e = 39 ± 18 keV and Δ e = 43 ± 14 keV.

The state determined from the transition (c) can be associated with two states: $E_x = 5153 \pm 8$ keV with $\Gamma \leq 20$ keV and $J^\pi = 3^-$ [20], and $E_x = 5106 \pm 8$ keV with $\Gamma = 45 \pm 2$ keV and $J^\pi = 2^+$ [24]. The energy difference is Δ e = +36 ± 19 keV and Δ e = -11 ± 19 keV.

The final overview of the results is presented in figure 7. All known states in ^{18}Ne are shown above the proton emission threshold up to 1.5 MeV. The observed two-proton transitions are drawn as discontinuous lines. It is interesting to observe that all lines are connected with a known state in ^{18}Ne, and inversely all known states above the proton emission threshold have been fed by a two-proton transition. Two states in ^{19}Na positioned very close to each other, at 5809 keV and 5815 keV, may be related to one unique state. In the mirror nucleus ^{19}O there are several states known at close energies, two of them may be the analogue states since they have large widths: Γ = 490 keV at $E_x = 5.54$ MeV with $J^\pi = \frac{3}{2}^+$, and Γ = 110 keV at $E_x = 6.120$ MeV with $J^\pi = \frac{3}{2}^+$. However, it is probable that the states determined in ^{19}Na from the two-proton emission result from the mixed combination of several broad states. In that hypothesis the two-proton emission happens up to the maximum energy available in the center of mass frame, which seems to be the case here.

Several aspects of the experiment has to be examined in the light of the new results:

– The non observation of two-proton decays from the compound nucleus ^{19}F in the measurement with the stable beam ^{18}O may be explained by the fact that other decay channels are open in that nucleus, mainly the alpha emission, with much larger branching ratios. They should have reduced drastically the two-proton contribution.
– As discussed above, in figure 3 the peaks B and C correspond to the detection of only one proton of the two-proton transitions. The efficiency to detected this kind of event is increased by focusing effects at forward angles. The focusing effects also exist in inelastic scattering with gamma emission. However simulations show that the focusing effect is higher when the total available energy is shared by two protons. This explains why we observe only the peaks B and C, corresponding to two-proton decays (p,pp), and not other peaks corresponding to inelastic (p,pγ) contributions. However, these inelastic contributions should be present in figure 3 with a lower intensity, and they may explain the small differences we can observe between the R-matrix calculation and the experimental result. An example of (p,pγ) contribution has been shown in fig-

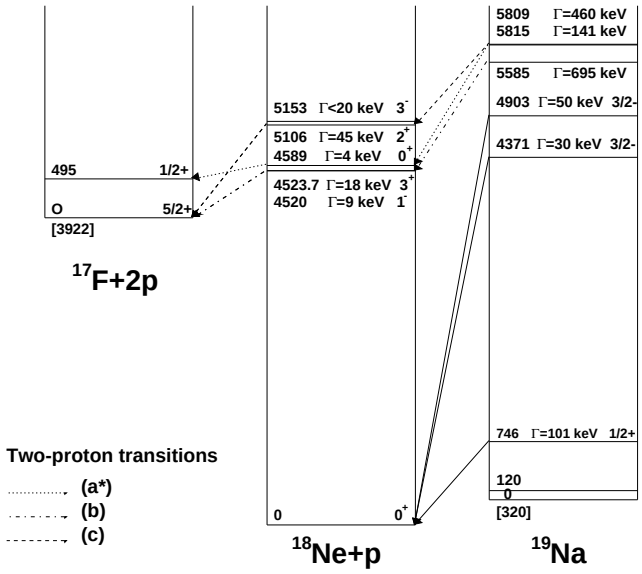

Fig. 7. Level scheme which summarizes the known states properties of ^{19}Na. All known unbound states above the proton emission threshold on ^{18}Ne are shown here up to 1.5 MeV. The observed two-proton transitions are shown with non continuous lines. They are all connected with known states in ^{18}Ne.

ure 4 for the inelastic scattering on the first excited state.

10 Three-proton, simultaneous two-proton emissions ?

The three-proton emission channel is open in our experiment but no event with 3 protons in coincidence has been observed. This does not mean they are not produced since our detection efficiency is very low for this kind of events. However, the probability to observe 2 of the 3 protons is much larger. In this case we should observe 3 two-proton coincidences. They are not observed in figure 6. But, it is possible that 2 of the 3 protons have energies very close, as it seems to be the case with the events of the transition labelled (c). In this case, they are not resolved, we only see twice two-proton coincidences. Our simulation of the process has shown that we never have enough energy in the center of mass frame to produce 3 proton transitions where two of them are detected with the energies we have measured. In conclusion, no three-proton emission was observed in our experiment.

In figure 6, it is surprising to observe that the transition labelled (c) is located near the line e1 = e2. For these events, the difference in energy is very small, the mean value for $|\overline{e1-e2}|_{lab}$ = 500 ± 370 keV and $|\overline{e1+e2}|_{lab}$ = 21200 ± 510 keV. These events may be related to the simultaneous emission of two protons (^{2}He emission) [23, 24]. The equality of the energies may be a natural consequence of this decay mode. However, we were not able to measure the angular distribution for these events because our angular acceptance was relatively narrow. Since the analysis of these events using the sequential decay mode involves an intermediate excited state in ^{18}Ne which is known, it is probable that the equality of the energies is just accidental.

11 Conclusions

We have performed an experiment to measure the elastic scattering excitation function of a ^{18}Ne radioactive beam from the SPIRAL facility on a thick solid cryogenic hydrogen target. We have observed two new states in the compound nucleus ^{19}Na with $J^\pi=\frac{3}{2}^-$, at E_x=4371 ± 10 keV with Γ=30 ± 10 keV and at E_x=4903 ± 10 keV with Γ=50 ± 10 keV. The understanding of the decay process was crucial to understand the high excitation energy part of the ^{19}Na excitation function. We have also observed two intense peaks mainly corresponding to the detection of single protons from two-proton emissions. A strip detector allowed to identify the two-proton transitions. It is important to notice that the detection of two-proton events is enhanced at forward angles from focusing effects in inverse kinematics. The two-proton events have been interpreted in a sequential decay mode, and three new states with large width may have been determined in ^{19}Na.

Future experiments of elastic scattering at low energy are possible even with much lower beam intensities. They will provide an efficient tool to undertake the spectroscopy of the most exotic nuclei. These future experiments aimed at the search of states at high excitation energies in the unbound neutron-deficient nuclei should take into account the detection of the multi-proton events and include proton detectors of high granularity and energy resolution. In addition, the improvement of the detection system by increasing the total acceptance and by measuring the angular distribution will allow the efficient spectroscopy of the intermediate states from multi-particle emissions, as it has been demonstrated in our experiment with the measurement of states in ^{18}Ne from two-proton emissions. However, it is important that future theoretical studies shed light on the two-proton emission from excited states, and particularly on the simultaneous emission mode.

12 Acknowledgement

We would like to thank the GANIL staff and the technical support for the successful challenge of providing for the first time the SPIRAL beam with good optical qualities. We thank M. Ploszajczak for stimulating discussions. This work has been supported by the European Community-Access to Research Infrastructure action of the Improving Human Potential Program, contract N° HPRI1999-00066.

References

1. S.M. Lukyanov, Yu. E. Penionzhkevich, R. Astabatyan, S. Lobastov, Yu. Sobolev, D. Guillemaud-Mueller, G. Faivre, F. Ibrahim, A.C. Mueller, F. Pougheon, O. Perru, O. Sorlin, I. Matea, R. Anne, C. Cauvin, R. Hue, G. Georgiev, M. Lewitowicz, F. de Oliveira Santos, D. Verney, Z. Dlouhy, J. Mrazek, D. Baiborodin, F. Negoita, C. Borcea, A. Buta, I. Stefan and S. Grevy, J. Phys. G. **28**, (2002) L41.
2. M. Notani, H. Sakurai, N. Aoi, Y. Yanagisawa, A. Saito, N. Imai, T. Gomi, M. Miura, S. Michimasa, H. Iwasaki, N. Fukuda, M. Ishihara, T. Kubo, S. Kubono, H. Kumagai, S.M. Lukyanov, T.K. Onishi, Yu.E. Penionzhkevich, S. Shimoura, T. Teranishi, K. Ue, V. Ugryumov, A. Yoshida, Phys. Lett. B **542**, (2003) 84.
3. T. Zerguerras, B. Blank, Y. Blumenfeld, T. Suomijrvi, D. Beaumel, B.A. Brown, M. Chartier, M. Fallot, J. Giovinazzo, C. Jouanne, V. Lapoux, I. Lhenry-Yvon, W. Mittig, P. Roussel-Chomaz, H. Savajols, J.A. Scarpaci, A. Shrivastava and M. Thoennessen, Eur. Phys. J. A, **20**, (2004) 389.
4. J. Cerny, R.A. Mendelson, G.J. Wozniak, J.E. Esterl and J.C. Hardy, Phys. Rev. Let. **22**, (1969) 612.
5. W. Benenson, A. Guichard, E. Kashy, D. Mueller, H. Nann and L.W. Robinson, Phys. Let. B **58**, (1975) 46.
6. D.R. Tilley, H.R. Weller, C.M. Cheves, R.M. Chasteler, Nucl. Phys. A **595**, (1995) 1.
7. C. Angulo, G. Tabacaru, M. Couder, M. Gaelens, P. Leleux, A. Ninane, F. Vanderbist, T. Davinson, P.J. Woods, J.S. Schweitzer, N.L. Achouri, J.C. Angélique, E. Berthoumieux, F. de Oliveira Santos, P. Himpe, and P. Descouvemont, Phys. Rev. C **67**, (2003) 014308.

8. L. Axelsson, M.J.G. Borge, S. Fayans, V.Z. Goldberg, S. Grevy, D. Guillemaud-Mueller, B. Jonson, K.-M. Kallman, T. Lonnroth, M. Lewitowicz, P. Manngård, K. Markenroth, I. Martel, A. C. Mueller, I. Mukha, T. Nilsson, G. Nyman, N. A. Orr, K. Riisager, G. V. Rogatchev, M.-G. Saint-Laurent, I. N. Serikov, O. Sorlin, O. Tengblad, F. Wenander, J. S. Winfield, and R. Wolski, Phys. Rev. C **54**, (1996) R1511.
9. V.Z. Goldberg, V.I. Dukhanov, A.E. Pakhomov, G.V. Rogachev, I.N. Serikov, M. Brenner, K-M. Källman, T. Lönnroth, P. Manngård, L. Axelsson, K. Markenroth, W. Trzaska and R. Wolski, Physics of Atomic Nuclei (Yadernaja Fizika) **60**, (1997) 1186.
10. K. Markenroth, L. Axelsson, S. Baxter, M.J.G. Borge, C. Donzaud, S. Fayans, H.O.U. Fynbo, V.Z. Golberg, S. Grévy, D. Guillemaud-Mueller, B. Jonson, K.-M. Källman, S. Leenhardt, M. Lewitowicz, T. Lönnroth, P. Manngard, I. Martel, A.C. Mueller, I. Mukha, T. Nilsson, G. Nyman, N.A. Orr, K. Riisager, G.V. Rogatev, M.-G. Saint-Laurent, I.N. Serkov, N.B. Shul'gina, O. Sorlin, M. Steiner, O. Tengblad, M. Thoennessen, E. Tryggestad, W. H. Trzaska, F. Wenander, J.S. Winfield, and R. Wolski, Phys. Rev. C **62**, (2000) 034308.
11. A.C.C. Villari, C. Barue, G. Gaubert, S. Gibouin, Y. Huguet, P. Jardin, S. Kandri Rody, F. Landre Pellemoine, N. Lecesne, R. Leroy, M. Lewitowicz, C. Marry, L. Maunoury, J.Y. Pacquet, J.P. Rataud, M.G. Saint-Laurent, C. Stodel, J.C. Angelique, N.A. Orr, R. Lichtenthaler, Nucl. Phys. A **701**, (2002) 476c.
12. A.C.C. Villari and the SPIRAL group, Nucl. Instr. and Meth. B **204**, (2003) 31.
13. W. Mittig and P. Roussel-Chomaz, Nuclear Physics A **693**, (2001) 495.
14. P. Dolégiéviez, P. Robillard, P. Gallardo, M. Ozille, D. Heuze, GANIL Report **A00 01**, (2000)
15. http://www.srim.org/
16. H. Orihara, G. Rudolf and Ph. Gorodetzky, Nucl. Phys. A **203**, (1973) 78.
17. E. Berthoumieux, B. Berthier, C. Moreau, J.P. Gallien, A.C. Raoux, Nucl. Instr. and Meth. B **136-138**, (1998) 55.
18. E.K. Warburton, B.A. Brown, Phys. Rev. C, (1992) 923.
19. B. A. Brown, A. Etchegoyen and W. D. M. Rae, MSU-NSCL report **N 524**.
20. K.I. Hahn, A. Garcia, E. G. Adelberger, P. V. Magnus, A. D. Bacher, N. Bateman, G. P. A. Berg, J. C. Blackmon, A. E. Champagne, B. Davis, A. J. Howard, J. Liu, B. Lund, Z. Q. Mao, D. M. Markoff, P. D. Parker, M. S. Smith, E. J. Stephenson, K. B. Swartz, S. Utku, R. B. Vogelaar, and K. Yildiz, Phys. Rev. C **54**, (1996) 1999.
21. A. Garcia, E. G. Adelberger, P. V. Magnus, D. M. Markoff, K. B. Swartz, M. S. Smith, K. I. Hahn, N. Bateman, and P. D. Parker, Phys. Rev. C **43**, (1991) 2012.
22. D.W. Bardayan, J.C. Blackmon, C.R. Brune, A.E. Champagne, A.A. Chen, J.M. Cox, T. Davinson, V.Y. Hansper, M.A. Hofstee, B.A. Johnson, R.L. Kozub, Z. Ma1, P.D. Parker, D.E. Pierce, M.T. Rabban, A.C. Shotter, M.S. Smith, K.B. Swartz, D.W. Visser, and P.J. Woods, Phys. Rev. Lett. **83**,(1999) 45.
23. V.I. Goldansky, Nuclear Physics **19**, (1960) 482.
24. J. Gómez del Campo, A. Galindo-Uribarri, J. R. Beene, C. J. Gross, J. F. Liang, M. L. Halbert, D. W. Stracener, D. Shapira, R. L. Varner, E. Chavez-Lomeli, M. E. Ortiz, Phys. Rev. Lett. **86**, (2001) 43.